

A STUDY OF AMMUNITION RESPONSE TO THE INTERIOR BALLISTICS ENVIRONMENT OF GUN LAUNCH

Stephen E. Ray*
Army High Performance Computing Research Center
Minneapolis, MN 55415

Michael J. Nusca
U.S. Army Research Laboratory
Aberdeen Proving Ground, MD 21005

Albert W. Horst
Business Plus Corporation
Aberdeen, MD 21001

ABSTRACT

A multidisciplinary modeling approach is used to study the dynamic response of a notional telescoped-ammunition projectile to gun chamber pressure dynamics generated by a densely packed solid propellant charge during gun launch. Since material stress imposed on the ammunition could potentially damage the projectile or its payload, a detailed knowledge of the peak stress is essential in the ammunition design process. The modeling approach begins with the Army's interior ballistics code ARL-NGEN3 predicting ignition, flamespreading and combustion of the solid propellant charge. Following this, the structural mechanics code EPIC simulates the response of the projectile to the pressure dynamics computed by the ARL-NGEN3 code. The results are analyzed in order to develop a comprehensive understanding of the in-bore behavior of the projectile.

1. INTRODUCTION

Gun-launched projectiles currently being used by the objective force as well as being designed for the future combat systems include smart/guided projectiles utilizing an onboard electronics suite and an internal propulsion unit (e.g., rocket), and those carrying high explosive payloads. In order to increase payload capacity, these ammunition configurations include long projectile afterbodies that intrude into the gun chamber or cartridge. Concurrently there is a requirement to maximize the muzzle exit velocity of these projectiles and therefore many charge designs call for densely packed solid propellant and the attendant high loading density (propellant mass divided by total initial volume of the chamber). The combination of this afterbody intrusion, a potentially sensitive payload, and densely-packed propellant results in a complex system that challenges munition designers and theoretical interior ballisticians alike.

A recent Army research effort involved development of a numerical methodology for studying these types of complex munitions systems using a multidisciplinary approach (Ray, et al., 2005). The work brought together two numerical models with different yet complementary capabilities: the U.S. Army's state-of-the-art interior ballistics (IB) code, ARL-NGEN3 (Gough, 1996; Gough, 1997; Nusca and Gough, 1998; Nusca, 2004), and EPIC, a prominent computational structural mechanics (CSM) code (Johnson, et al., 2003).

The ARL-NGEN3 code is a multidimensional, multiphase computational fluid dynamics (CFD) code capable of including the three-dimensional geometry of the charge, the gun, and the projectile in the interior ballistics simulation. It uses a coupled Eulerian-Lagrangian approach in order to capture the continuous and discrete components of the flowfield. The continuous phase contains the gases generated by the reaction of the igniter and the propellant and is modeled using the Eulerian-based continuum flow solver (CFS). The discrete components include the unreacted parts of the charge and are simulated using the Lagrangian-based large particle integrator (LPI).

The EPIC code is a Lagrangian-based finite element solid mechanics code. Among its many features include the ability to model a solid using elements or meshless particles for high-deformation problems (Johnson, et al., 2000; Johnson, et al., 2002). It has been used extensively in penetration mechanics applications because of its ability to compute damage done to a material and the phenomena resulting from the failure and breaking of the material (Holmquist and Johnson, 2005).

In previous work (Nusca and Horst, 2003; Ray, et al., 2005), the coupled modeling approach was used to study the flamespread of a notional telescoped-ammunition round and the dynamic response of the projectile. Figure 1 shows a sketch of the combustion chamber behind and

Report Documentation Page

*Form Approved
OMB No. 0704-0188*

Public reporting burden for the collection of information is estimated to average 1 hour per response, including the time for reviewing instructions, searching existing data sources, gathering and maintaining the data needed, and completing and reviewing the collection of information. Send comments regarding this burden estimate or any other aspect of this collection of information, including suggestions for reducing this burden, to Washington Headquarters Services, Directorate for Information Operations and Reports, 1215 Jefferson Davis Highway, Suite 1204, Arlington VA 22202-4302. Respondents should be aware that notwithstanding any other provision of law, no person shall be subject to a penalty for failing to comply with a collection of information if it does not display a currently valid OMB control number.

| | | | | | |
|--|------------------------------------|--|---|---------------------------------|---------------------------------|
| 1. REPORT DATE 01 NOV 2006 | 2. REPORT TYPE N/A | 3. DATES COVERED - | | | |
| 4. TITLE AND SUBTITLE A Study Of Ammunition Response To The Interior Ballistics Environment Of Gun Launch | | 5a. CONTRACT NUMBER | | | |
| | | 5b. GRANT NUMBER | | | |
| | | 5c. PROGRAM ELEMENT NUMBER | | | |
| 6. AUTHOR(S) | | 5d. PROJECT NUMBER | | | |
| | | 5e. TASK NUMBER | | | |
| | | 5f. WORK UNIT NUMBER | | | |
| 7. PERFORMING ORGANIZATION NAME(S) AND ADDRESS(ES) Army High Performance Computing Research Center Minneapolis, MN 55415 | | 8. PERFORMING ORGANIZATION REPORT NUMBER | | | |
| 9. SPONSORING/MONITORING AGENCY NAME(S) AND ADDRESS(ES) | | 10. SPONSOR/MONITOR'S ACRONYM(S) | | | |
| | | 11. SPONSOR/MONITOR'S REPORT NUMBER(S) | | | |
| 12. DISTRIBUTION/AVAILABILITY STATEMENT Approved for public release, distribution unlimited | | | | | |
| 13. SUPPLEMENTARY NOTES See also ADM002075., The original document contains color images. | | | | | |
| 14. ABSTRACT | | | | | |
| 15. SUBJECT TERMS | | | | | |
| 16. SECURITY CLASSIFICATION OF: | | | 17. LIMITATION OF ABSTRACT UU | 18. NUMBER OF PAGES 8 | 19a. NAME OF RESPONSIBLE PERSON |
| a. REPORT unclassified | b. ABSTRACT unclassified | c. THIS PAGE unclassified | | | |

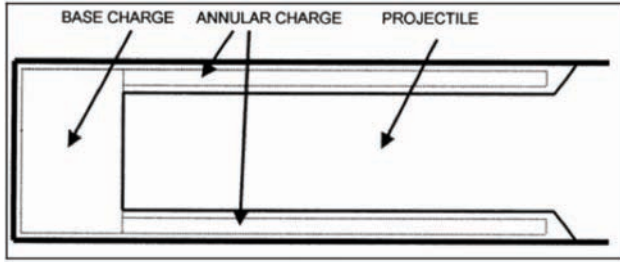


Figure 1. Sketch of the chamber and projectile tail in the notional round (Nusca and Horst, 2005).

around the tail of the projectile. In the ARL-NGEN3 simulations, the use of propellant grains in the main charge resulted in strong pressure waves moving axially through the chamber, growing particularly strong when they reflected off of the chamber. Using the computed pressure in the chamber as a driver, the EPIC simulations showed the dynamic response of the projectile, including the vibratory load on a notional payload.

2. INTERIOR BALLISTICS SIMULATIONS

Recent work (Nusca and Horst, 2005; Williams, et al., 2005) began a coordinated experimental and computational effort focusing on validation of the coupled modeling approach and subsequent exploration of the capabilities of this combined experimental/numerical IB research. The experimental effort (Williams, et al., 2005) involves a series of experiments being conducted at the U.S. Army Research Laboratory using a highly instrumented projectile mounted in a clear-chamber ballistics simulator. Figure 2 shows a schematic of the test fixture. The geometry of the combustion chamber is axisymmetric, and the ignitor is located along the centerline. The points labeled “P” and “S” indicate the location of pressure and strain gauges, respectively. The focus of the experimental tests is the flamespread and projectile response during the early part of the firing cycle, so the projectile is pinned to prevent motion during the tests. Part of the chamber wall is designed to rupture at a prescribed pressure to end each test.

Included in the experimental tests are two different propellant configurations, shown in the top two sketches in Figure 3. The propellant used in each configuration is 19-perforation, partially-cut JA2 stick propellant. In the “rear loading” configuration, only the region behind the projectile tail is filled with propellant, while in the “shell loading” configuration, propellant is placed only the annular region between the projectile and the chamber wall extending to the chamber base. In each of the configurations, an identical amount of propellant, about 3 kg, is used.

The ARL-NGEN3 simulations looked at the two configurations from the experimental tests plus a third in

which all of the combustion chamber is filled with the same JA2 stick propellant, called the “full loading” configuration. The code cannot currently model the partially-cut stick propellant geometry directly but can approximate it quite well by assuming that all of the propellant is 19-perforated JA2 grain with the axial interphase drag nulled (i.e. the gas can move unobstructed in the axial direction).

Figure 4 shows the computed pressure from the ARL-NGEN3 simulations at three axial locations along the chamber’s outer wall: near the breech, midway along the chamber, and near the barrel end of the chamber, 6 cm, 28 cm, and 50 cm respectively from the chamber breech face. In each picture in Figure 4, the blue line is the pressure difference between the forward and rear locations; the oscillations in these lines indicate the formation of pressure waves of moderate amplitude moving axially through the chamber. The oscillations first appear especially early in the shell-

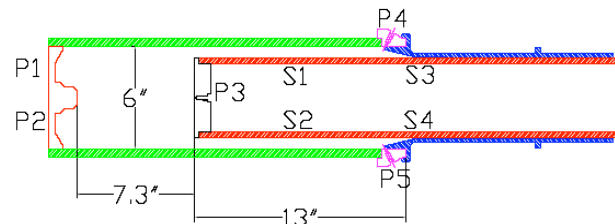


Figure 2. Geometry used in the simulations. In the experiment, the green material is polymethyl methacrylate, which ruptures before projectile motion (projectile shown in red). In the simulations, this surface is assumed never to rupture, in order to study the effects of projectile motion (Williams, et al., 2005).

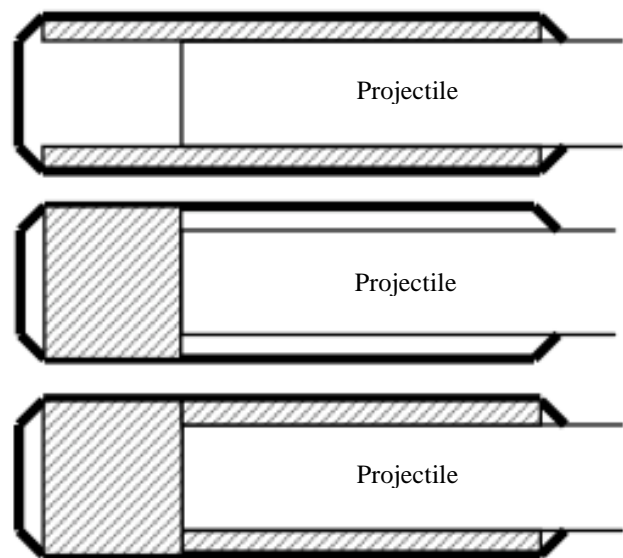


Figure 3. Sketch of the shell loading configuration (top), rear loading configuration (middle), and full loading configuration (bottom). The thatched area signifies the location of the propellant charge (Nusca and Horst, 2005).

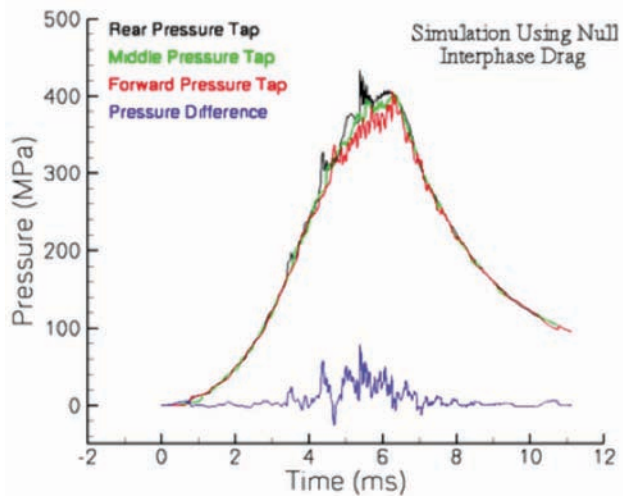
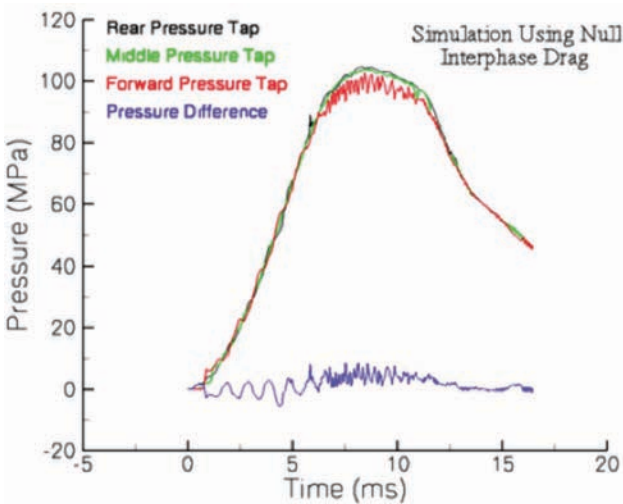
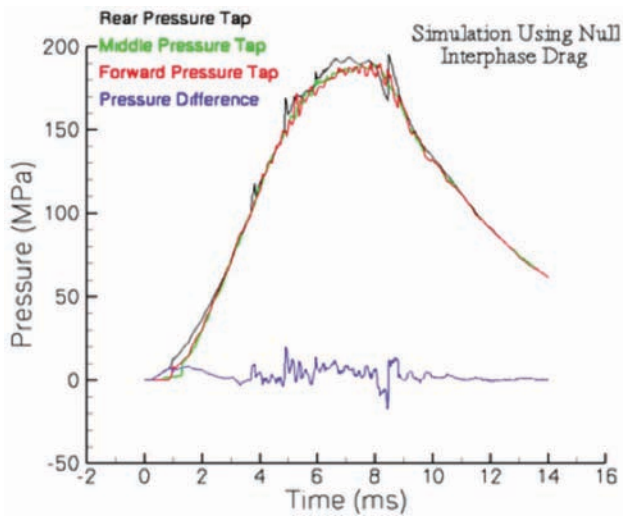


Figure 4. Pressure computed at three axial locations in the combustion chamber by ARL-NGEN3: rear loading (top), shell loading (middle), full loading (bottom). The blue line shows the difference in pressure between the forward station and the rear station (Nusca and Horst, 2005).

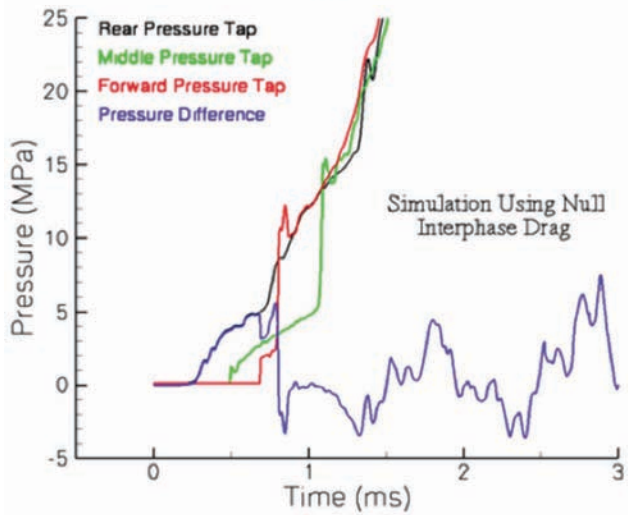
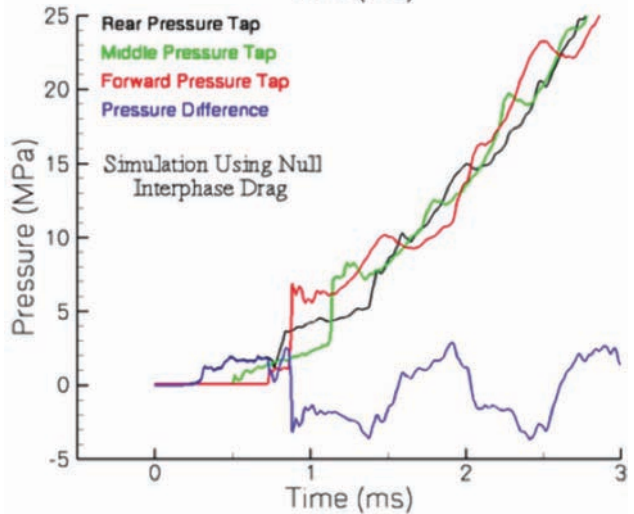
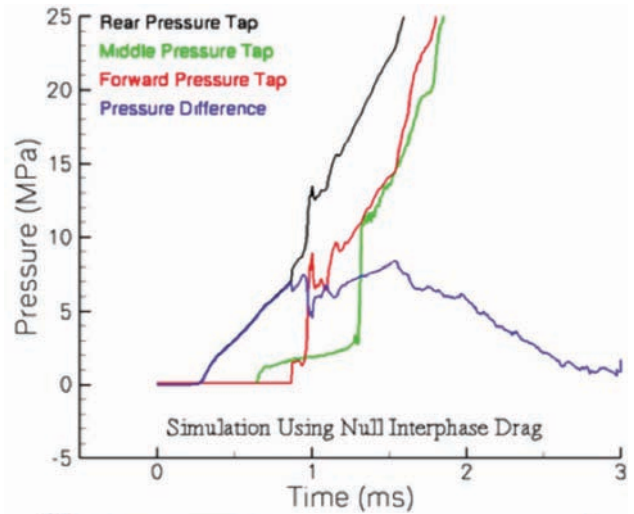


Figure 5. Pressure computed at three axial locations in the combustion chamber by ARL-NGEN3: rear loading (top), shell loading (middle), full loading (bottom). The positioning of the propellant closer to the igniter in the rear-loading and full-loading configurations cause faster pressure rise in those cases (Nusca and Horst, 2005).

loading configuration. The focus of the experimental effort is the early part of the firing cycle, and so Figure 5 shows, for each picture in Figure 4, a blow up of the time and pressure range of interest (0-3 ms and 0-25 MPa).

The line plots shown in Figures 4 and 5 do not show the highest pressure occurring in the combustion chamber. Referring again to the sketches in Figure 3, the thick black lines indicate the chamber wall in each sketch. When the pressure waves strike the chambrage (shown as the right end of the thick black lines), the convergence of the chambrage and the projectile surface causes the highest pressure in this region. Figure 6 shows the pressure at 1 ms into the shell-loading simulation. The three axial locations used for the line plots of Figures 4 and 5 are denoted “R”, “M”, and “F”. Figure 6 shows that the highest pressure at that time instance is fore of the “F” location and under the chambrage.

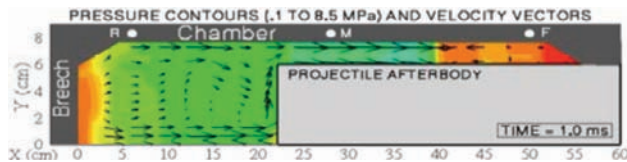


Figure 6. Pressure and velocity vectors in the simulation of the shell-loading configuration. Note that the radial axis is expanded for clarity (Nusca and Horst, 2005).

3. PROJECTILE DYNAMIC RESPONSE

3.1 Rear-Loading Configuration

The top pictures in Figures 4 and 5 show the pressure in the rear-loading simulation. With no propellant loaded between the projectile tail and the chamber wall, no reaction takes place in that region to strengthen pressure waves. While pressure waves move axially to and from the chambrage, they remain relatively weak. A result of that can be seen in Figure 5, where the difference between the pressure at the rear tap and the pressure at the front tap remains non-negative until past 3 ms and does not go strongly negative until 8 ms, by which time the projectile is well down the gun barrel. During this and the other simulations presented in this report, only the first 4.8 ms of the firing cycle were simulated, because the experiments to be run will end well before that point in time.

Figure 7 shows the pressure on the projectile at three times in the simulation. Since the ARL-NGEN3 simulations were run assuming axisymmetry, the pressure driving the EPIC simulation is also axisymmetric. The sharp change of the projectile color to blue partway along the projectile indicates the location where the chambrage

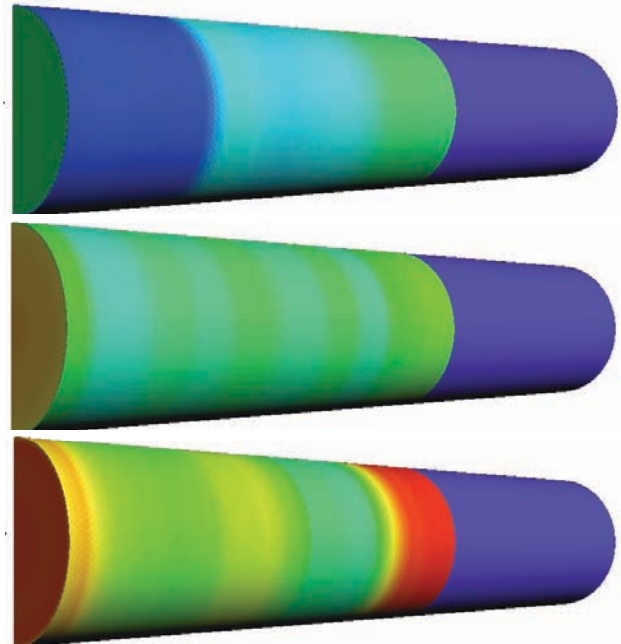


Figure 7. Pressure on the projectile at 1.0 ms, 1.25 ms, and 1.5 ms into the rear-loading simulation. The bands of varying colors are indicative of pressure waves moving axially through the chamber. The maximum and minimum pressures in these pictures are 0 and 24 MPa.

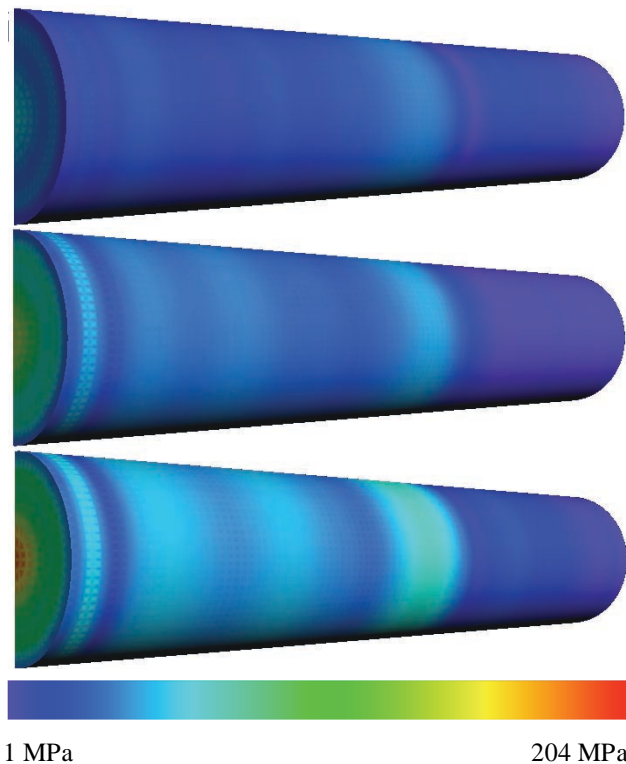


Figure 8. Von Mises stress in the projectile at 1.0 ms, 1.25 ms, and 1.5 ms into the rear-loading simulation. The light blue band in all three pictures shows that high stress occurs at the same axial location as the chambrage.

meets with the projectile surface. This is an effect of the assumption that no hot gas goes between the projectile and the gun tube wall. In the bottom picture of Figure 7, notice that the highest pressure on the surface of the projectile is at the barrel end and is caused by the reflection of a pressure wave off of the chambrage.

Figure 8 shows the resulting von Mises stress in the projectile at the same time instances as those in Figure 7, i.e. 1.0 ms, 1.25 ms, and 1.5 ms. As was expected, there is a strong correlation between the locations of regions of high pressure in Figure 7 and the locations of regions of high stress in Figure 8. The highest stress that can be seen on the outer surface is in the center of the tail face. This high stress is caused by a combination of the pressure imposed on the back face pushing axially, and the pressure pushing on the outer edge of the back face, compressing the face radially.

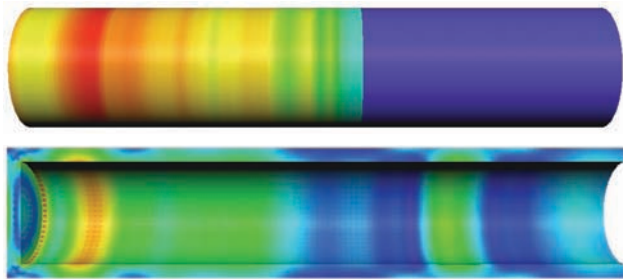


Figure 9. Pressure (top) and von Mises stress (bottom) in the projectile at 4.8 ms into the rear-loading simulation. The peak pressure at this time is 195 MPa, and the peak stress is 1.4 GPa.

Some stress waves are also seen moving fore of where the chambrage meets with the projectile surface. This can be seen more clearly in Figure 9, which shows the pressure and stress at 4.8 ms into the simulation. The von Mises stress is shown on the inside surface of the hollow projectile; the stress is higher on the inner surface because the projectile is in compression. There are several high-stress bands fore of the chambrage showing stress waves moving axially and indicating that the pressure input excited several modes of vibration of the projectile, causing it to “ring.” The highest stress is about 1.4 GPa, which is in the neighborhood of the yield stress for a number of high-strength steels.

A fast Fourier transform (FFT) of the pressure imposed midway between the chambrage and the end of the projectile during the first 4 ms of the firing cycle shows that there is a very low-frequency oscillation in the input pressure, which is the overall rise and fall of pressure during the firing cycle. Beyond that, there are a large number of peaks in the FFT graph, none of them very high, perhaps indicating that there are a lot of small oscillations in the input pressure arising from small combustion instabilities as opposed to a pressure mode of

the chamber being excited. In fact, although it is not obvious from Figures 4 and 5, the pressure arising from this loading configuration is far richer in terms of pressure oscillations than the other two cases. While the shell-loading and the full-loading cases have strong pressure oscillations in the neighborhood of 1 kHz, they have no other strong oscillations to speak of.

The graph of an FFT of the acceleration of one point in the projectile tail also shows a large number of little peaks, most of them forced frequencies from the oscillations in the pressure. Several large peaks are seen at about 5 kHz, 10 kHz, 12 kHz, 15.5 kHz, 20 kHz, and 21.2 kHz, and these likely are natural frequencies or overtones of natural frequencies. This case shows far more projectile vibration than the other two cases, owing to the elevated level of pressure oscillations compared with the other cases. This type of analysis is important when studying the survivability of a vibration-sensitive payload.

3.2 Shell-Loading Configuration

The middle pictures in Figures 4 and 5 show the pressure in the shell-loading simulation. In this loading configuration, the propellant is loaded between the projectile tail and the chamber wall instead of behind the projectile tail. Because the propellant on average is further from the igniter, the pressure rise rate is lower, and the overall shape of the pressure-time curve is shorter in pressure but wider in time (compare the top and middle pictures in Figure 4, noting that the scales of each plot are

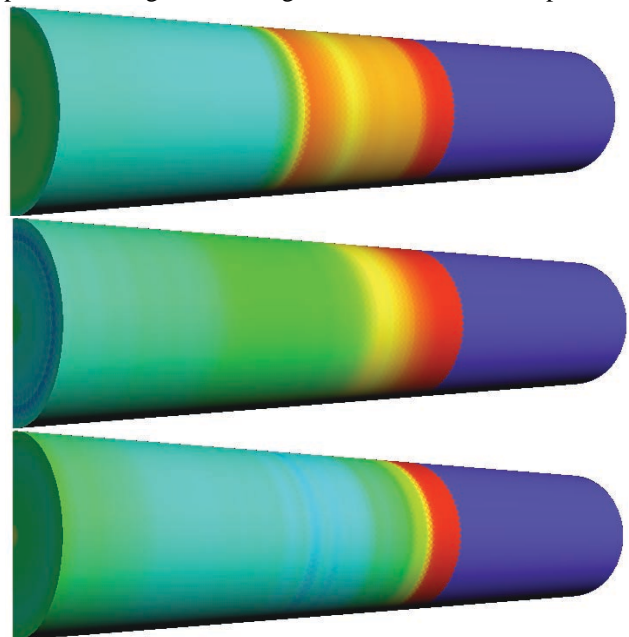


Figure 10. Pressure imposed on the projectile at 1.0 ms (top, 0-8.9 MPa shown), 1.5 ms (middle, 9-14 MPa shown), and 2.0 ms (bottom, 17-20 MPa shown) into the shell-loading simulation.

different). The difference between the pressure at the rear tap and the pressure at the front tap first goes negative before 1 ms and then does so repeatedly for much of the firing cycle. An FFT of the pressure imposed midway between the chambrage and the end of the projectile during the first 4 ms of the simulation shows 1.2 kHz oscillations, which are the strong oscillations visible between about 2 and 6 ms in Figure 4, and no strong higher-frequency signals. While there are small higher frequency oscillations visible in Figure 5, there are no strong high-frequency modes.

Figure 10 shows the pressure imposed on the projectile by the shell-loaded propellant at three times. The pictures show the motion of pressure waves as they move axially in the annulus between the projectile and the chamber wall. The presence of such waves is never desirable but can especially be problematic when the annulus is packed with propellant. A locally high pressure results in a local increase in burn rate, further strengthening the pressure front. That there is a constant outer diameter of the projectile means that projectile motion provides no local volume increase in the annulus and so no release of the locally high pressure.

The top picture in Figure 10 shows the return of the first pressure front after reflection off of the chambrage. In all three pictures, the pressure is higher near the chambrage than at any other point on the projectile

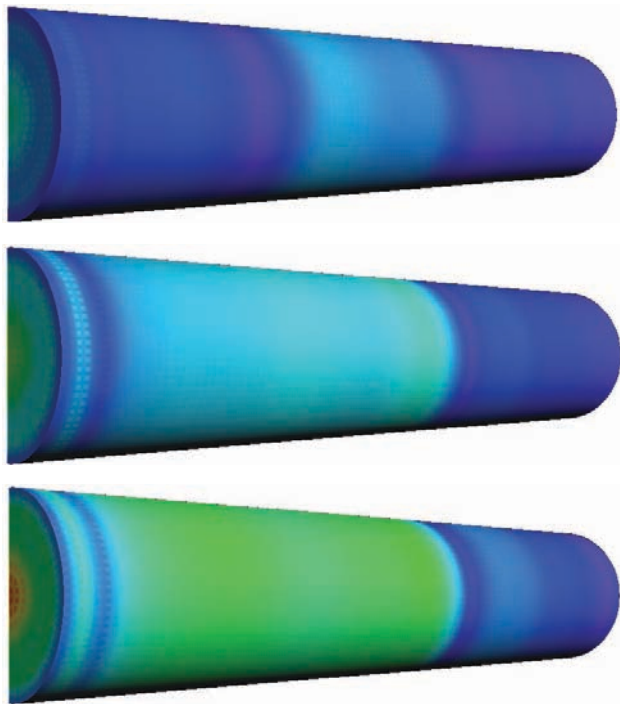


Figure 11. Von Mises stress in the projectile at 1.0 ms (top), 1.5 ms (middle), and 2.0 ms (bottom) into the shell-loading simulation. In all pictures, the minimum and maximum stress shown are 1 MPa and 128 MPa.



Figure 12. Von Mises stress in the projectile at 4.8 ms into the shell-loading simulation. The peak stress at this time is 705 MPa and occurs at the center of the rear face of the projectile.

surface. At 2.0 ms, the pressure is also elevated at both ends of the annular region.

In looking at the response of the projectile, an analysis of the von Mises stress, pressure, and acceleration at various points in the projectile shows a number of vibrational modes. Vibrations near 1.2 kHz are forced by the oscillations in the pressure input. Natural modes with frequencies of 9.5 kHz and 18 kHz are excited fairly strongly, while smaller vibrations near 5 kHz, 12 kHz, 15.5 kHz, and 25 kHz are also seen.

Figure 11 shows the von Mises stress at the same three times as in Figure 10. Again, the location of areas of higher stress track well with the higher input pressure in Figure 10. It is interesting to note that the pressure waves forward of the chambrage are weaker in this case than in the rear-loading case. This can be seen by comparing Figure 12 with Figure 9, both of which show the von Mises stress at 4.8 ms into the simulations. In the shell-loading case (Figure 12), not only is the peak stress lower, but there are also no higher stress bands visible in the front part of the projectile. This occurs because of the absence in this case of high-frequency oscillations in the computed pressure and thus no excitation of longitudinal vibrational modes.

3.3 Full-Loading Configuration

The bottom pictures in Figures 4 and 5 show the pressure in the full-loading simulation. This simulation, while not planned to be part of the series of experiments to be performed at ARL, is closer in design to a fielded round, in which the entire combustion chamber is initially filled with propellant. Comparing the top and bottom pictures in Figure 4, the initial pressure rise is comparable to that in the rear-loading configuration, which is expected because the propellant loading in the neighborhood of the igniter is the same. The presence of propellant between the projectile tail and the chamber wall, however, strengthens the pressure waves moving to the chambrage, so that when the first pressure wave strikes the chambrage at about 0.8 ms, the pressure at the forward pressure tap exceeds that at the rear pressure tap, a condition that occurs repeatedly during the firing cycle.

An FFT of the pressure imposed on the projectile shows oscillations near 1 kHz and 2 kHz, but the overall

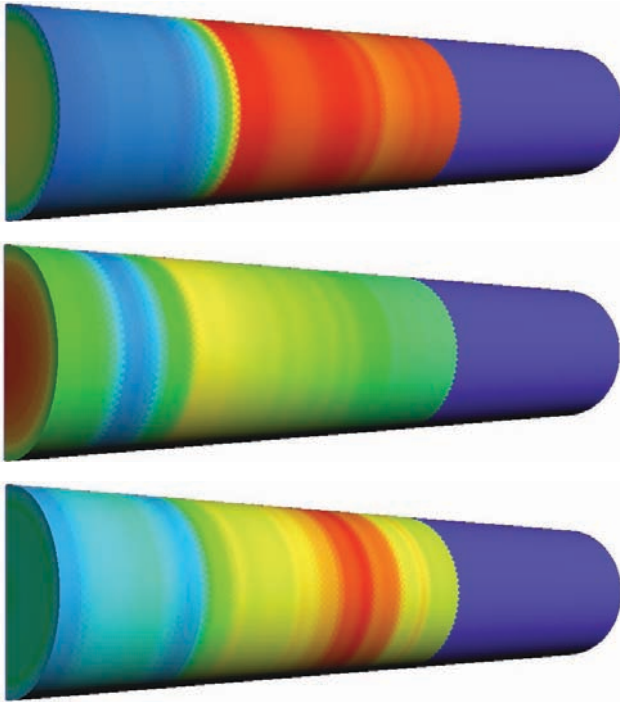


Figure 13. Pressure imposed on the projectile at 1.0 ms (top, 3-12.7 MPa shown), 1.25 ms (middle, 14-20 MPa shown), and 1.5 ms (bottom, 23-27 MPa shown) into the full-loading simulation.

plots of the FFT from this case and from the shell-loading case look similar, perhaps indicating that the presence of propellant in the annulus tends to prevent the excitation of higher-frequency pressure modes in addition to strengthening the 1 kHz mode.

Figure 13 shows the pressure imposed on the projectile in the full-loading simulation at three times. Again, the pictures show the motion of pressure waves moving axially between the rear of the projectile and the chamber. The presence of propellant in the annulus combined with the overall increase in the amount of propellant in the system make the pressure waves very strong.

Figure 14 shows the von Mises stress at the same times as those used in Figure 13. The stress is much higher in this case, reaching 238 MPa by 1.5 ms into the firing cycle. There are waves moving axially through the projectile, but the higher stress in Figure 14 makes them difficult to see. Figure 15 shows the stress at 4.8 ms into the firing cycle. The large red area shows where the stress exceeds the yield stress of the steel and indicates that the projectile likely would fail in a gun firing of this charge configuration.

An analysis of the vibrational response of the projectile shows, in addition to the forced frequencies,

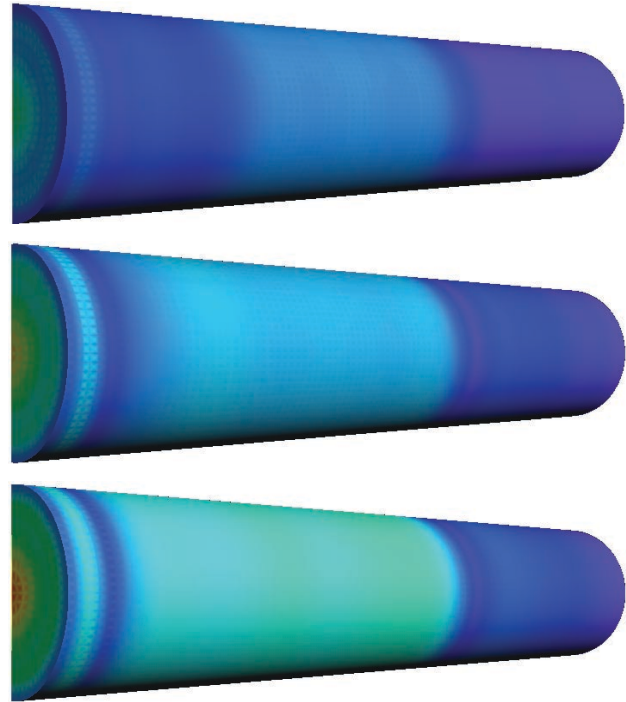


Figure 14. Von Mises stress in the projectile at 1.0 ms (top), 1.25 ms (middle), and 1.5 ms (bottom) into the full-loading simulation. In all pictures, the minimum and maximum stress shown are 1 MPa and 238 MPa.

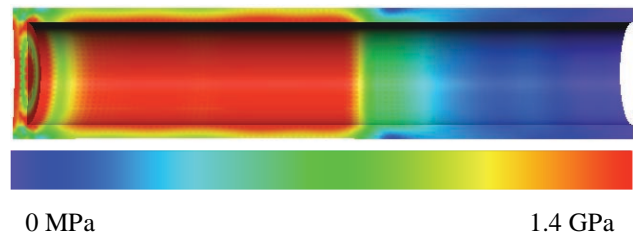


Figure 15. Von Mises stress in the projectile at 4.8 ms into the full-loading simulation. The peak stress at this time is over 3.3 GPa. The region in red shows where the stress has surpassed 1.4 GPa, which is roughly the yield stress of a number of high-strength steels.

strong frequencies near 5 kHz, 9.5 kHz, 12 kHz, and 25 kHz. There does appear also to be oscillations near 10.3 kHz; this is the only case that seemed to excite two separate vibration modes near 10 kHz.

CONCLUSIONS

A multidisciplinary modeling approach was used to study the dynamic response of a notional telescoped-ammunition projectile to gun chamber pressure dynamics. The approach used the ARL-NGEN3 code to predict the interior ballistics phenomena. The results from ARL-

NGEN3 were used as input by the EPIC code to drive a simulation of the dynamic response of the projectile. The results of this modeling effort will be compared with experimental results to quantify the accuracy of this numerical approach. Several test problems were simulated and analyzed, including a study of vibrations in the projectile.

ACKNOWLEDGMENTS

The research reported in this document was performed in part in connection with contract DAAD19-03-D-0001 with the U.S. Army Research Laboratory. The AHPCRC and the DoD MSRC (ARL) supplied computing time.

REFERENCES

- Gough, P.S., 1996: Modeling Arbitrarily Packaged Multi-Increment Solid Propellant Charges of Various Propellant Configurations, *Proc. of the 33rd JANNAF Combustion Meeting*, CPIA Publication 653, vol. 1, 421-435.
- Gough, P.S., 1997: Extensions to the NGEN Code: Propellant Rheology and Container Properties, *Proc. of the 34th JANNAF Combustion Meeting*, CPIA Publication 662, vol. 3, 265-281.
- Holmquist, T.J. and Johnson G.R., 2005: Characterization and Evaluation of Silicon Carbide for High-Velocity Impact, *J. Appl. Phys.*, **97**, 093502.
- Johnson, G.R., Beissel, S.R., and Stryk, R.A., 2000: A Generalized Particle Algorithm for High Velocity Impact Computations, *Comp. Mech.*, **25**, 245-256.
- Johnson, G.R., Beissel, S.R., and Stryk, R.A., 2002: An Improved Generalized Particle Algorithm That Includes Boundaries and Interfaces, *Intl. J. Num. Meth. Eng.*, **53**, 875-904.
- Johnson, G.R., Beissel, S.R., Stryk, R.A., Gerlach, C.A., and Holmquist, T.J., 2003: *User Instructions for the 2003 Version of the EPIC Code*, Air Force Research Laboratory Contract Report F08630-02-M-0077, October 2003.
- Nusca, M.J., 2004: *High Performance Computing and Simulation for Advanced Armament Propulsion*, US Army Research Laboratory, Aberdeen Proving Ground, MD, ARL-TR-3215, June 2004.
- Nusca, M.J. and Gough, P.S., 1998: *Numerical Model of Multiphase Flows Applied to Solid Propellant Combustion in Gun Systems*, AIAA Paper No. 98-3695, July 1998.
- Nusca, M.J. and Horst, A.W., 2003: Progress in Multidimensional, Two-Phase Simulations of Notional Telescoped-Ammunition Solid Propelling Charge, *Proceedings of the 39th JANNAF Combustion Meeting*, CPIA Publication JSC CD-25, December 2003.
- Nusca, M.J. and Horst, A.W., 2005: *Progress in Modeling Ignition in a Solid Propellant Charge for Telescoped Ammunition*, US Army Research Laboratory, Aberdeen Proving Ground, MD, ARL-TR-3673, November 2005.
- Ray, S.E., Nusca, M.J., and Newill, J.F., 2005: *A Study of Projectile Response to Ballistics Environment*, US Army Research Laboratory, Aberdeen Proving Ground, MD, ARL-TR-3672, November 2005.
- Williams, A., Colburn, J., Howard, S., Brant, A., Nusca, M., Ray, S., and Horst, A., 2005: Full-Scale Simulator Studies of a Notional Telescoped-Ammunition Charge, *Proc. of the 40th JANNAF Combustion Subcommittee Meeting*, CPIA Publication JSC CD-39, June 2005.